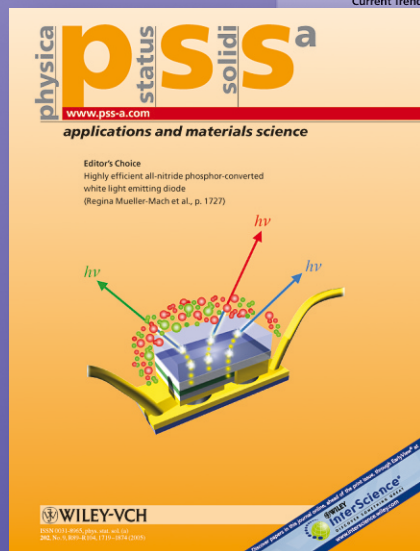


# physica p status solidi S S

[www.interscience.wiley.com](http://www.interscience.wiley.com)

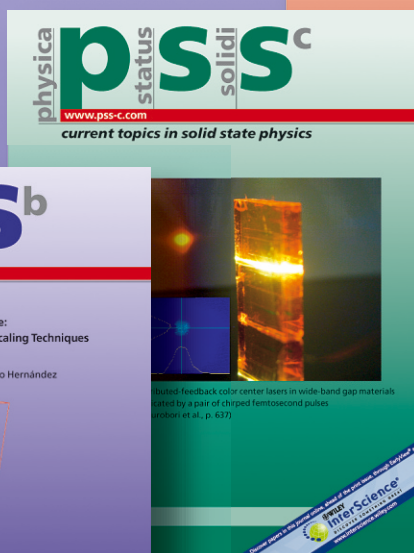
reprints



[www.pss-a.com](http://www.pss-a.com)



[www.pss-b.com](http://www.pss-b.com)



[www.pss-c.com](http://www.pss-c.com)



[www.pss-rrl.com](http://www.pss-rrl.com)

# Structural and optical properties of zinc oxide nanopowders doped with Mn

M. Ebrahimizeh Abrishami, S. M. Hosseini\*, E. Attaran Kakhki, and A. Kompany

Department of Physics (Materials and Electroceramics Laboratory), Ferdowsi University of Mashhad, Iran

Received 19 September 2009, revised 16 November 2009, accepted 6 December 2009

Published online 8 April 2010

**Keywords** ZnO, nanoparticles, sol-gel process, structure, optical properties

\* Corresponding author: e-mail sma\_hosseini@yahoo.com, Phone: +98-511-8435723, Fax: +98-511-8796426

Pure ZnO and  $Zn_{1-x}Mn_xO$  ( $x=0, 0.02, 0.06, 0.10, 0.15$ ) nanopowders have been synthesized by sol gel technique at low temperatures. XRD results indicate that the powder has a hexagonal polycrystalline structure without secondary phases. The nanopowders were characterized using the X-ray diffraction (XRD) and transmission electron microscopy

(TEM) observation. Kramers-Kronig's analysis of mid-IR reflectance spectra were employed to determine the doping effect on the optical constants and optical phonon modes frequencies. The optical band gap energy decreases from 3.22 eV to 3.12 eV for pure ZnO and  $Zn_{0.9}Mn_{0.1}O$  dispersed powders, respectively.

© 2010 WILEY-VCH Verlag GmbH & Co. KGaA, Weinheim

**1 Introduction** Zinc oxide is an n-type II-VI semiconductor most stably crystallized in wurtzite structure. The space group is  $P63mc$  and lattice constants are  $a=3.25 \text{ \AA}$  and  $c=5.21 \text{ \AA}$  [1]. Due to its remarkable electrical and optical characteristics such as large direct band gap energy (3.34 eV), controllable conductivity, ceramics properties ZnO based materials technologically has a unique potential to be applied in thermoelectric [2], optoelectronic [3], piezoelectric [4] and varistors [5]. Furthermore, ZnO is considered for spintronics applications with magnetic ions (Co, Ni, V, Fe and Mn) doping. For this reason, Mn doping has valuable spin off in electrical, optical and magnetic properties of ZnO. In this direction, Mn doped ZnO has become a reasonable choice for Diluted Magnetic Semiconductors (DMS). Even, ferromagnetic state was reported below and above room temperature [6, 7]. In addition to magnetic properties of ZnO:Mn, Mn can severely affect the electrical properties especially in ceramics due to Mn preferring to place in grain boundaries [8]. For example, the nonlinear coefficient of ZnO varistors is increased suddenly by Mn doping [9]. The nonlinearity of varistor ceramics coefficient may improve using nanosized particle as it greatly depends on homogeneity of microstructure.

However, in recent years, synthesis of nanopowders of ZnO, MnO and doping ZnO with transition metals by different routes such as wet chemical methods like sol-gel [10], co-precipitation [11], and combustion [12] in nanotechnology has occurred worldwide.

In this paper, we have synthesized pure and doped ZnO nanopowders via sol gel technique. Effect of Mn

doping in lattice parameters were investigated. Dispersion parameters such as refractive index, extinction coefficient and phonon modes frequencies were determined by analyzing the reflectance spectra in mid-IR region. An absorbance spectrum in UV region was applied to estimate the optical band gap energy. The effect of Mn on varistor behavior of ZnO ceramics is also studied.

**2 Experimental procedures** The precursors for the synthesis of  $Zn_{1-x}Mn_xO$  ( $x=0.00, 0.02, 0.06, 0.10$  and  $0.15$ ) nanoparticles were zinc acetate dehydrate,  $Zn(CH_3COO)_2 \cdot 2H_2O$ , manganese acetate tetrahydrate,  $Mn(CH_3COO)_2 \cdot 4H_2O$ , acetic acid and diethanolamine (DEA). Zinc and appropriate amount of manganese acetate were dissolved in a mixture of isopropanol and distilled water by magnetic stirring, heating at  $40 \text{ }^\circ\text{C}$  for 30 minutes. Then the mixture contained acetic acid and DEA was added to clear cations solution and constantly stirred for 10 min to obtain a clear solution. The molar ratios of acetic acid and DEA to cations kept to unity, respectively. Afterwards, the solution with  $\text{pH}=7$  was refluxed for 4 h at  $110^\circ\text{C}$  to obtain a clear sol. The gel was obtained with the help of heat bath at temperature of  $80 \text{ }^\circ\text{C}$  and then dried at temperatures of  $140\text{--}150 \text{ }^\circ\text{C}$ . The resultant powders were calcinated at  $400 \text{ }^\circ\text{C}$  for 2 h in air to prepare nanopowders.

Phase identification of nanopowders was analyzed by X-ray diffraction using  $\text{CuK}_\alpha$  radiation ( $\lambda=1.54056 \text{ \AA}$ ). Transmission electron microscopy (TEM, model: LEO 912AB-Germany) and scanning electron microscopy (SEM, model: LEO 1450VP-Germany) were used to

determine the particle size and morphology of nanopowders. Optical characterizations were carried out by Fourier transform infra red spectroscopy from reflectance spectra of powders in KBr matrix in the region (400-4000  $\text{cm}^{-1}$ ) and also by UV absorbance spectra from nanopowders ultrasonically dispersed in distilled water were recorded as discussed by Bangal *et al.* [13].

### 3 Results and discussion

**3.1 Structure and particle size** The crystal structure, plane orientations and lattice constants were analyzed from XRD patterns as shown in Fig. 1. The crystal structure of  $\text{Zn}_{1-x}\text{Mn}_x\text{O}$  ( $x=0.00, 0.02, 0.06, 0.10, 0.15$ ) was wurtzite with preferred orientation along [101] direction for all samples. Furthermore, XRD spectra revealed mono-phasic structure even in heavy doped nanopowders. This increasing Mn solubility in ZnO structure is due to decreasing particle size, as discussed by Straumal *et al.* [8, 14].

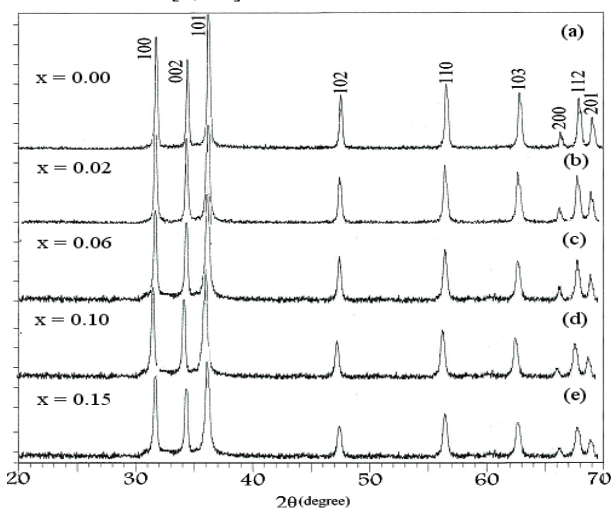


**Figure 1** XRD patterns for  $\text{Zn}_{1-x}\text{Mn}_x\text{O}$  (a)  $x=0.00$ , (b)  $x=0.02$ , (c)  $x=0.06$ , (d)  $x=0.10$  and (e)  $x=0.15$ .

Mn effect on lattice constants and peak positions shifts is presented in Fig. 2. As Mn content increases up to

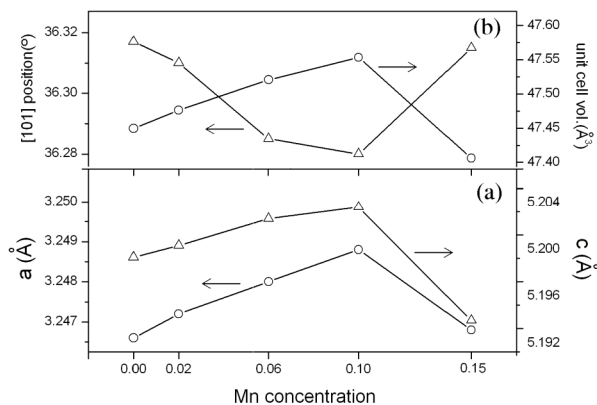


**Figure 2** Structural properties of undoped and doped samples, (a) lattice constants, (b) relation between unit cell volume and angle of [101] peak positions.

0.10, the reflection peaks slightly shift to lower angle. Typically, the angles related to [101] peaks are mentioned in Fig. 2b. In fact, increasing the lattice constants ( $a$  and  $c$ ) and the unit cell volume cause the shift in peaks position to lower angles [15]. Because of higher radius of  $\text{Mn}^{2+}$  (0.66 Å), in comparison with  $\text{Zn}^{2+}$  (0.60 Å), increasing the lattice constants are expectable.

However, we observed that the peak positions of  $\text{Zn}_{0.85}\text{Mn}_{0.15}\text{O}$  shifted towards higher angles (Fig. 2b). Thus, we may conclude that the lattice constants decreased (Fig. 2a) for the following reason. Manganese can also exist in  $\text{Mn}^{3+}$ ,  $\text{Mn}^{4+}$  in addition to  $\text{Mn}^{2+}$ . The ionic radii of  $\text{Mn}^{3+}$  (0.58 Å) and  $\text{Mn}^{4+}$  (0.53 Å) are smaller than  $\text{Zn}^{2+}$ . In doped ZnO substitution of  $\text{Zn}^{2+}$  by  $\text{Mn}^{3+}$  and  $\text{Mn}^{4+}$  brings about the lattice constant decrease as noted by Bhatti *et al.* [16]. In addition, XRD spectra indicates that full width at half maximum (FWHM) of [101] peak has decreased with increasing Mn content which is deduced as decreasing particle size, confirmed by Scherrer relation. SEM and TEM images are shown in Fig. 3a and 3b and the average of particle size is estimated to be about 30-40 nm in diameters.

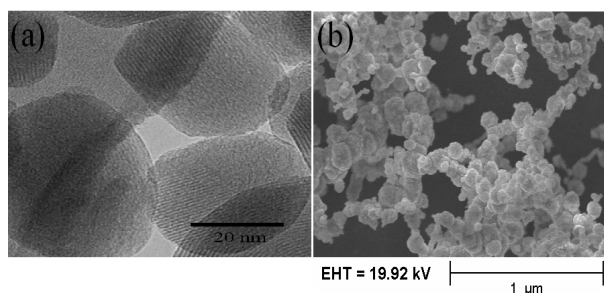


**Figure 3** (a) TEM and (b) SEM image of  $\text{Zn}_{0.98}\text{Mn}_{0.02}\text{O}$  nanopowder.

### 3.2 Optical properties

**3.2.1 FTIR analysis** The mid-IR reflectance spectra of pure and doped ZnO nanopowders are shown in Fig. 4. There is a strong reflection between longitudinal and transversal phonon modes frequencies ( $\omega_{\text{TO}}$  and  $\omega_{\text{LO}}$ ), the region reststrahlen. Weak reststrahlen band reflection in  $\text{Zn}_{0.85}\text{Mn}_{0.15}\text{O}$  is dominated by high free carrier concentration due to heavily doping level. A sharp falling in reflectance spectra around  $\omega_{\text{LO}}$  indicates the semi-insulating system in this region. Also the reststrahlen band becomes wider in doped samples with increasing Mn content up to 0.10 results in more space between phonon modes frequencies. However, this phenomenon acts vice versa in  $\text{Zn}_{0.85}\text{Mn}_{0.15}\text{O}$  samples. In addition, the high frequencies region is dominated by valence electrons which are observed in Fig. 4. In this case no extra electrons are added to system in doped samples respect to undoped ZnO except in heavily doped ( $x=0.15$ ) nanopowders in which the high frequencies reflectance is remarkably increased. Likewise, we concluded these results as Zn ions substitutions by Mn ions from XRD analysis.

If the reflectance  $R(\omega)$  is generally recognized in all frequencies, then the refractive index  $n(\omega)$ , extinction coefficient  $k(\omega)$  and dielectric function can be obtained by Kramers-Kronig's dispersion relations as follows [17]:

$$n(\omega) = \frac{1 - R(\omega)}{1 + R(\omega) - 2 \cos \varphi(\omega) \sqrt{R(\omega)}} \quad (1)$$

$$k(\omega) = \frac{2 \sin \varphi(\omega) \sqrt{R(\omega)}}{1 + R(\omega) - 2 \cos \varphi(\omega) \sqrt{R(\omega)}} \quad (2)$$

where  $\varphi(\omega)$  is the phase of reflectance wave. Figure 5 presents the changes of  $n(\omega)$  and  $k(\omega)$  versus wavenumber. The results indicated that the high frequency refractive in  $Zn_{0.85}Mn_{0.15}O$  increased due to sudden change in reflectance spectra. Moreover, the phonon modes frequencies can be easily obtained. The dielectric function  $\varepsilon(\omega) = \varepsilon'(\omega) + i\varepsilon''(\omega)$  is controlled by contributions from phonons and charge carriers. The real part of dielectric function  $\varepsilon'(\omega)$  is negative between longitudinal and transverse phonon modes frequencies. The phonon modes frequencies can be deduced from  $\varepsilon'(\omega) = n^2(\omega) - k^2(\omega)$  by determining the intersections of  $n(\omega)$  and  $k(\omega)$  curves. The values of  $\omega_{TO}$  and  $\omega_{LO}$  for pure and doped ZnO nanostructures are summarized in Table 1.

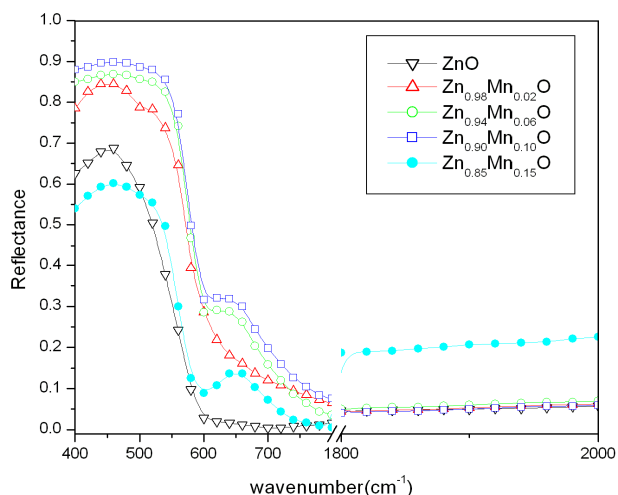


**Figure 4** Reflectance spectra in mid-IR region of undoped and Mn doped ZnO nanopowders.

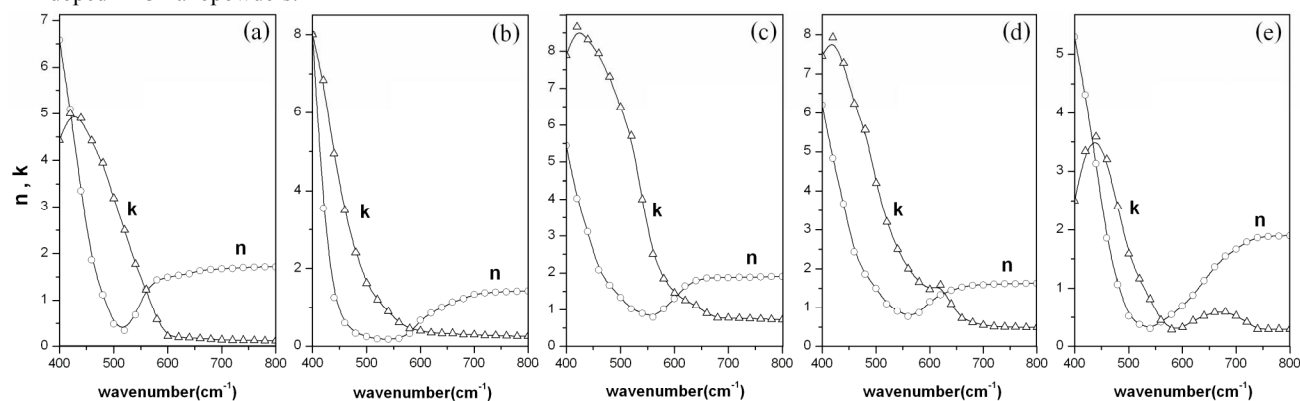


**Figure 5** The refractive index and extinction coefficient of (a) ZnO and  $Zn_{1-x}Mn_xO$ : (b)  $x=0.02$ , (c)  $x = 0.06$ , (d)  $x=0.10$  and (e)  $x=0.15$ .

**Table 1** Lattice-dynamical parameters of pure and doped ZnO nanopowders calculated at 400 °C.

Mn content	Present work					Others			
	0.00	0.02	0.06	0.10	0.15	0.00[18]	0.00[19]	0.00[20]	0.10[20]
TO mode	419.32	401.27	390.00	373.00	429.30	377	410	383	360
LO mode	559.26	580.71	605.00	619.12	560.95	577	591	538	541

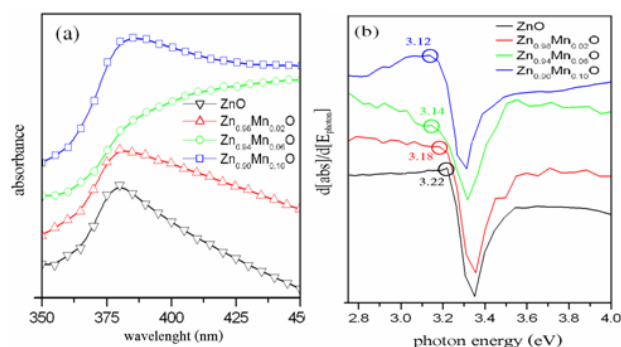


**Figure 6** (a) Optical absorbance spectra of  $Zn_{1-x}Mn_xO$  and (b) first derivative of absorbance in terms of photon energy (the band gap energies are circularly marked in the figure).

**3.2.2 UV analysis** The UV absorbance spectra of pure and Mn-doped ZnO nanopowders are shown in Fig. 6a. A characteristic absorption peak is evident for all UV spectra. The absorption peaks in Fig. 6 shift to longer wavelengths as Mn content increases.

It must be noted that the absorbance behavior is completely different from the thin films due to scattering process of the ultraviolet wave from particles dispersed in water.

Since the size of the nanoparticles dispersed in water is much smaller than incident light wavelength, the absorbance spectra are approvable to determine the optical band gap energy,  $E_g$ . As shown in Fig. 6b, a reasonable method for extracting band gap energy is investigation of the maxima in the first derivative of absorbance with respected to photon energy spectra at the lower energy sides [21]. The band gap decreases from 3.22 eV to 3.12 eV as Mn content increases from  $x=0.0$  to  $x=0.10$ . Decreasing band gap energy with increasing lattice parameters is a well known behavior as discussed theoretically by Wunderlich *et al.* [22].

**4 Conclusion** Single phase pure and Mn doped ZnO nanopowders have been synthesized using sol gel technique, calcinated at 400 °C, with crystalline size about 30-40nm in diameters. Lattice constants are increased and the optical band gap energy decreased as Mn concentration rises up to  $x=0.10$  in conformity to inverse relation between them. The optical band gap energy decreases from 3.22 eV to 3.12 eV for pure ZnO and  $Zn_{0.9}Mn_{0.1}O$  dispersed powders, respectively. The phonon modes frequencies have been deduced from intersections of  $n(\omega)$  and  $k(\omega)$  curves.

## References

- [1] E. H. Kisi and M. M. Elcombe, *Acta. Cryst.* **45**, (1989) 1867-1870 (1989).
- [2] M. Ohtaki, K. Araki, and K. Yamamoto, *J. Electron. Mater.* **38**, 1234-1238 (2009).
- [3] V. A. Fonoberov and A. A. Balandin, *J. Nanoelectron. Optoelectron.* **1**, 19-38 (2006).
- [4] S. S. Kwon, W. K. Hong, G. Jo, J. Maeng, T. W. Kim, S. Song, and T. Lee, *Adv. Mater.* **20**, 4557-4562(2008).
- [5] S. T. Kuo and W. H. Tuan, *J. Am. Ceram. Soc.* **91**, 1572-1579 (2008).
- [6] R. K. Singhal, M. Dhawan, S. Kumar, S. N. Dolia, Y. T. Xing, and E. Saitovitch, *Physica B* (2009), doi:10.1016/j.physb.2009.07.100.
- [7] M. Ebrahimizadeh Abrishami, S. M. Hosseini, E. Attaran Kakhki, A. Kompany, and M. Ghasemifard, *Int. J. Nanosci.* (2009), accepted.
- [8] B. Straumal, B. Baretzky, A. Mazilkin, S. Protasova, A. Myatiev, and P. Straumal, *J. Europ. Ceram. Soc.* **29**, 1963-1970 (2009).
- [9] Y. W. Hong and J. H. Kim, *Ceram. Int.* **30**, 1301-1306 (2004).
- [10] Q. Xu, S. Zhou, and H. Schmidt, *J. Alloys Compd.* (2009), DOI: 10.1016/j.jallcom.2009.08.033.
- [11] R. S. Yadav, A. C. Pandey, and S. S. Sanjaya, *Chalcogenide Lett.* **6**, 233-239 (2009).
- [12] N. Riahi-Noori, R. Sarraf-Mamoory, P. Alizadeh, and A. Mehdikhani, *J. Ceram. Process. Res.* **9**, 246-249 (2008).
- [13] M. Bangal, S. Ashtaputre, S. Marathe, A. Ethiraj, N. Hebalkar, S. W. Gosavi, J. Urban, and S. K. Kulkarni, *Hyperfine Interactions* **160**, 81-94 (2005).
- [14] W. Lojkowski, A. Gedanken, E. Grzanka, A. Opalinska, T. Strachowski, R. Pielaszek, A. Tomaszewska-Grzeda, S. Yatsunenko, M. Godlewski, H. Matysiak, and K.J. Kurzydowski, *J. Nanopart. Res.* (2008), DOI: 10.1007/s11051-008-9559-9.
- [15] S. Karamat, S. Mahmood, J. J. Lin, Z. Y. Pan, P. Lee, T. L. Tan, S. V. Springham, R. V. Ramanujan, and R. S. Rawat, *Appl. Surf. Sci.* **254**, 7285-7289 (2008).
- [16] K. P. Bhatti, S. Chaudhary, D. K. Pandya, and S. C. Kashyap, *Solid State Commun.* **136**, (2005) 384-388.
- [17] F. Stern, *Solid State Phys.* **15**, 327-340 (1963).
- [18] P. Y. Emelie, J. D. Phillips, B. Buller, and U. D. Venkateswaran, *J. Electron. Mater.* **35**, 525-529 (2006).
- [19] Ashkenov, B. N. Mbenkum, C. Bundesmann, V. Riede, M. Lorenz, D. Spemann, E. M. Kaidashev, A. Kasic, M. Schubert, M. Grundmann, G. Wagner, H. Neumann, V. Darakchieva, H. Arwin, and B. Monemar, *J. Appl. Phys.* **93**, 126-133 (2003).
- [20] C. J. Cong, L. Liao, Q. Y. Liu, J. C. Li, and K. L. Zhang, *Nanotechnology* **17**, 1520-1526 (2006).
- [21] A. E. Morales, E. S. Mora, and U. Pal, *Revista Mexicana de Físicas* **53**, 18-22 (2007).
- [22] W. Wunderlich, L. Miao, M. Tanemura, S. Tanemura, P. Jin, K. Kaneko, A. Terai, N. Nabatova-Gabin, and R. Belkada, *Int. J. Nanosci.* **3**(4-5), 439-445 (2004).